Nuclear Physics B125 (1977) 349–368

A MEASUREMENT OF THE POLARIZATION PARAMETER IN LARGE ANGLE PROTON-PROTON ELASTIC SCATTERING AT 7.9 GeV/c

D.G. ASCHMAN *, D.G. CRABB, K. GREEN **, C. McDOWELL ***, P.M. PHIZACKLEA ‡, G.L. SALMON and T.O. WHITE ‡‡
Nuclear Physics Laboratory, Oxford University, Keble Road, Oxford, UK

J. ANTILLE, L. DICK, A. GONIDEC ‡‡‡, A. GSPONER + and M. WERLEN
CERN, Geneva, Switzerland

K. KURODA ★, A, MICHALOWICZ ★, D. PERRET-GALLIX ★ and M. POULET ★
Division des Hautes Energies, Institut de Physique Nucleaire, 91 Orsay, France

Received 5 April 1977
(Revised 16 May 1977)

The polarization parameter in proton-proton elastic scattering has been measured at an incident momentum of 7.9 GeV/c and four-momentum transfers in the range $0.9 < |t| < 6.5$ (GeV/c)^2 using a high intensity unpolarized proton beam incident on a polarized proton target. The angle and momentum of the forward scattered protons were measured with a magnet spectrometer and scintillation counter hodoscopes and the angle of the recoil proton was measured using similar hodoscopes. A clean separation between the elastic scattering from free hydrogen and that coming from inelastic interactions and from interactions with complex nuclei in the target was obtained. The polarization shows substantial structure rising from zero at $|t| = 1.0$ (GeV/c)^2 to a maximum at $|t| = 1.7$ (GeV/c)^2 and then falling to zero at $|t| = 2.0$ (GeV/c)^2. There is evidence of a further peak at $|t| = 2.8$ (GeV/c)^2. Above $|t| = 3.25$ (GeV/c)^2 the polarization is small and consistent with zero. A comparison of these data with data obtained at other beam momenta shows that the polarization parameter has a strong momentum dependence.

* Present address: Physics Department, Princeton University, Princeton, N.J. USA.
** Present address: Rutherford Laboratory, Chilton, Didcot, Oxon, UK.
*** Present address: Logica Ltd. 64 Newman St., London W1A 4SE, UK.
‡ Present address: CEGB, Leatherhead, Surrey, UK.
‡‡ Present address: Cavendish Laboratory, Cambridge University, Cambridge, UK.
‡‡‡ Present address: SLAC, P.O. Box 4349, Stanford, Ca 94305, USA.
+ Present address: ETH, Zurich Switzerland.
★ Present address: LAPP BP709, 74019 Annecy-le-vieux, France.

1. Introduction

In this article we present the results of an experiment which measured the polarization parameter in pp elastic scattering at 7.9 GeV/c carried out at the proton synchrotron NIMROD at the Rutherford Laboratory. The measurements covered large c.m. scattering angles between 30° and 86° corresponding to a four-momentum transfer range $0.94 < |t| < 6.1$ (GeV/c)^2.

The measurement of the spin-related parameters in pp elastic scattering has been much extended in the past few years to high beam momenta and measurements of the polarization parameter (P_0) have been extended out to large values of momentum transfer. The existing data show that there is significant structure in P_0 as a function of t, the four-momentum transfer squared, and that large values of P_0 exist at incident beam momenta up to at least 17.5 GeV/c.

Several measurements [1–3,6] in the region 1 to 6 GeV/c and $|t| \lesssim 1.0$ (GeV/c)^2 showed the development of a dip around $|t| = 0.7$ (GeV/c)^2. The experiments of Borghini et al. [4,5] were the first to extend the measurements to high beam momenta and subsequently to high t. These measurements at 6, 10, 12, 14 and 17.5 GeV/c showed that the dip at $|t| = 0.7$ (GeV/c)^2 evolved into a double zero as the incident momentum increased and that further structure existed at larger t. Above 6 GeV/c the dominant features of $P_0(t)$ are a peak at around $|t| = 0.3$ (GeV/c)^2 whose value decreases rapidly with the incident proton momentum, a double zero around $|t| = 0.7$ (GeV/c)^2 rising to a peak at $|t| = 1.7$ (GeV/c)^2 whose value is independent of the momentum. Finally P_0 again falls to zero around $|t| = 2.0$ (GeV/c)^2.

It is well known that changes in the structure of amplitudes in two-body reactions can lead to changes in the slope of the differential cross section but in general show up more dramatically in the polarization parameter which is an interference between the spin flip and non-flip amplitudes. In pp elastic scattering this correlation is evident as the differential cross section varies smoothly up to a beam momentum of 7 GeV/c and then develops a shoulder at $1 < |t| < 2$ (GeV/c)^2 between 7 and 12 GeV/c. This structure grows with increasing momentum until at an equivalent ISR momentum (1500 GeV/c) there is a significant dip near $|t| = 1.4$ (GeV/c)^2 followed by a broad peak around $|t| = 2.0$ (GeV/c)^2. At present there is no unique theoretical explanation for these effects. Some Regge-type models [9,11] give a reasonable description of the polarization data only for $|t| \lesssim 1.5$ (GeV/c)^2. Eikonal [12] and optical models [13,14] give a better overall description over a larger $|t|$ range, but pure optical models predict the polarization in pp and pn elastic scattering to be the same contrary to the data of Diebold et al. [15].

The aim of this experiment was to measure the polarization parameter over as wide a c.m. scattering angle range as possible, with good statistical accuracy, to provide a map of the structure for tests of the underlying amplitudes in pp elastic scattering. Also a measurement at 7.9 GeV/c provides a good intermediate link between the structure at 12.3 GeV/c with the relatively featureless data around 5 GeV/c, in a region where the differential cross section is changing quite significantly.

2. Experimental apparatus and procedures

The measurement of pp elastic scattering used a specially constructed beam (P81) from NIMROD which gave intensities of about 10^9 protons per pulse at 7.91 GeV/c [16] onto a standard CERN polarized proton target. The forward scattered protons were detected by scintillation and Cerenkov counters and the scattering angle and momentum determined by scintillation counter hodoscopes and a bending magnet. The recoil protons were detected by two trigger counters and their scattering angle measured by scintillation hodoscopes. The hodoscope data was sent to an on-line computer (Data General Nova 1220) which performed a simple on-line analysis and wrote the raw data onto magnetic tape.

2.1. The beam

The beam was obtained by parasitic extraction from the normal X3 extracted beam. The beam momentum was 7.88 GeV/c at the start of the flat-top but was ramped by 0.7% over the period of the beam spill to give an average beam momentum of 7.91 GeV/c. Since no detectors could be used to detect individual particles in such a high intensity beam, a small spot and small divergence and small halo were needed to keep the spatial variation of a beam particle within narrow limits.

NIMROD uses a plunge magnet extraction system for the X3 beam. A second plunge magnet was used to intercept a percentage of the beam destined for X3 and divert it in a single turn to the P81 extraction channel. With 3×10^{12} protons circulating in NIMROD and a 25% share of X3 the P81 beam delivered 1.0×10^9 protons per pulse with divergence ±0.55 mrad horizontally and ±0.7 mrad vertically into a spot size (FWHM) of 3 mm vertically and 4 mm horizontally. The intensity of the halo was 10^{-3} of peak intensity at a distance of 4 mm from the centre of the spot.

Although initial adjustments to the beam line were made with a scintillating screen and TV camera and polaroid film, the operation was much simplified by the addition of a multi-wire ionization chamber which displayed the beam size and position each pulse. The beam intensity was measured each pulse by a parallel plate ionization chamber. For the final adjustments a detailed measurement of the final focus was made by scanning a 1 mm thick copper target across the beam and viewing it with a counter telescope.

Later in the experiment, it was necessary to use other conditions at the final focus because of radiation damage to the polarized target. This will be discussed in more detail below.

2.2. The polarized target and radiation damage

A standard CERN target of the type described by Roubeau et al. [17] was used. The target material was 1-2 propanediol doped with Cr^V complexes and maintained

at a temperature of 0.5 K in a vertical magnetic field of 2.5 Tesla. The propanediol, in the form of small spheres of 1.5 mm diameter, filled a cylindrical cavity of diameter 16 mm and length 45 mm with packing fraction of about 0.7.

The overall polarization of the sample was measured by an NMR coil wrapped around the outside of the target. The NMR readout was controlled by the on-line computer and the area under the NMR signal was calculated digitally at the end of each accelerator pulse and the polarization calculated by scaling from the previously measured thermal equilibrium signal. The number was written to tape and to disk to enable the time dependence of the polarization value to be displayed on request. Also displayed was the NMR signal itself.

Initial polarization values obtained from this target system were generally in the range 70–75%. After exposure to a beam flux of 10^9 protons per pulse the initial polarization value ($P_{T,max}$) gradually decreases because of radiation damage. This decrease can be described by a simple exponential form

$$P_T(\phi) = P_{T,max}\, e^{-(\phi/\phi_0)} ,$$

where ϕ = integrated beam flux (proton · cm^{-2}), and ϕ_0 is the characteristic value. The effect has been studied previously with butanol targets in intense electron and photon beams [18] and ethyl glycol targets in proton beams [19] and values for ϕ_0 have been found in the range 2 to 5×10^{14} particle · cm^{-2}.

The NMR signal in the present experiment was derived from a coil wrapped around the outside of the target material and thus the NMR polarization value was an average over the target volume or a 'bulk' value. This may differ considerably from the value in the central core region ('core' value) from where the scattering is taking place so either the bulk value has to be corrected, or a direct measurement of the core value is necessary. If the beam spot is very small the frequency with which the target material has to be annealed or changed becomes high.

We tried to reduce the effects of radiation damage by spreading the beam over a larger cross section of the target by simply increasing the spot size (big beam) or by ramping the beam vertically during the spill. For each of these conditions we made a more direct measurement of the fall of core polarization by measuring the asymmetry in pp elastic scattering at $|t| = 1.7$ (GeV/c)^2. At this value of $|t|$ the asymmetry is high (15% for $P_T = 1$) and the trigger rate was 5 events per 10^9 incident protons. Pairs of spin up/spin down runs at this t setting were interspersed with normal data taking and the fall off of this asymmetry used in correcting the NMR value for the target polarization.

Fig. 1 shows the NMR target polarization estimate and the $|t| = 1.7$ asymmetry as a function of total beam through the target for the three beam conditions. Table 1 gives the parameters of the beam and I_0 (the $1/e$ value) in each case for both the NMR and asymmetry measurement.

It is interesting to speculate that the area of radiation damage consists of two regions, a central core which is damaged by the direct beam and a second area around the core which is damaged by secondary ionizing radiation. In each case

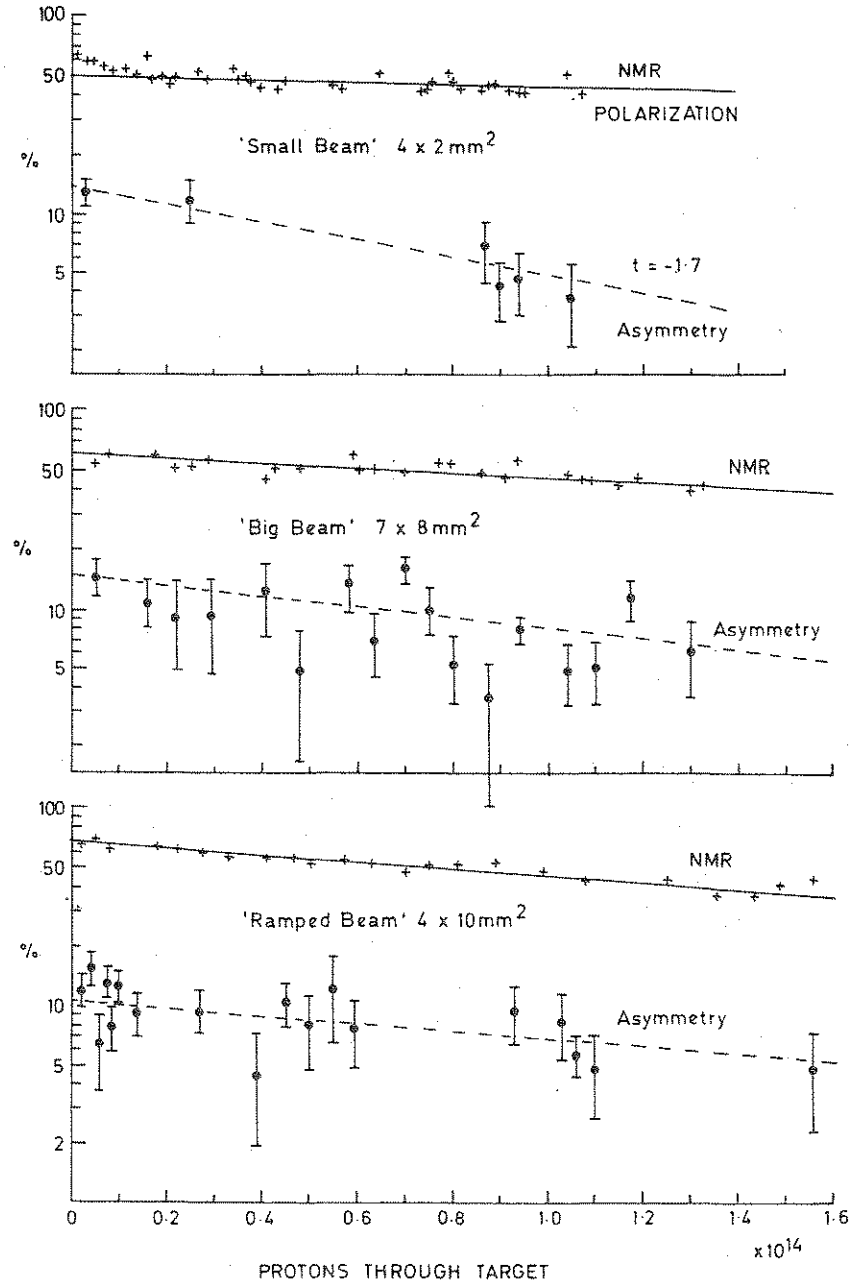

Fig. 1. The effect of radiation damage in the polarized target shown as the reduction of target polarization as a function of the total number of protons through the target for the three beam conditions described in the text. The reduction is shown for the two methods of measurement; an NMR method and a scattering asymmetry measurement.

Table 1
Radiation damage parameters for three beam conditions

Beam description and size	I_0 ($\times 10^{14}$ protons)		ϕ_0 10^{14} proton · cm^{-2}
	NMR	Asymmetry	
'Small' 4×2 mm^2	1.4	1.0 ± 0.1	2.2 ± 0.2
'Big' 8×7 mm^2	1.8	1.8 ± 0.2	2.2 ± 0.2
'Ramped' 4×10 mm^2	2.5	2.5 ± 0.2	2.5 ± 0.2

the damaged area was assumed to consist of a central core defined by the beam size (FWHM) and an outer ring of estimated width 0.7 cm. The value of ϕ_0 was calculated for each case and is given in the last column of table 1.

The average characteristic value for radiation damage to propanediol by 8 GeV/c protons is $\phi_0 = (2.2 \pm 0.25) \times 10^{14}$ protons · cm^{-2}. Attempts to anneal the target by heating to 185°K were not successful so that the target material was changed approximately every three days when the polarization had dropped to 50% or to a level such that the correction factor it was necessary to apply to the NMR value was a maximum of 15%. Most of the data was taken with the ramped beam.

2.3. The spectrometer

The layout of the apparatus is shown in fig. 2. An ionization chamber (IC) measured the beam intensity and the multiwire ionization chamber (MWIC) monitored the profile and position of the beam each pulse. The scattered and recoil proton trajectories were measured by scintillation counter hodoscopes, H_1 to H_9. Hodoscopes H_2 to H_9 had a spatial resolution of 3 mm while that of H_1 was 2 mm [24].

The forward spectrometer measured the production angle and momentum of the fast forward scattered proton. After emerging from the field of the polarized target

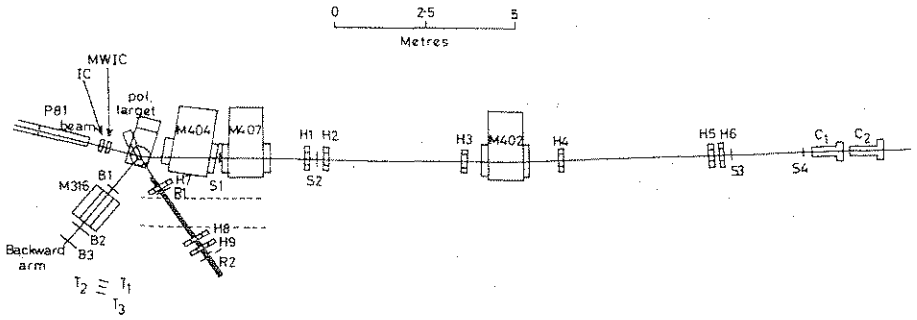

Fig. 2. Layout of the experiment.

magnet the proton was steered by magnets M_{404} and M_{407} towards the centre of the momentum analysing magnet M_{402}. The field in M_{402} was adjusted such that a proton at the centre of the acceptance (for any t value) emerged along a fixed line through the centres of counters S_3 and S_4. The one-metre long M_{402} provided, at maximum current, a $\int B dl$ of 1.8 Tesla metres giving a momentum resolution $\delta P/P$ of 2.0%. A detailed floating-wire study was made of the forward spectrometer as a check on the calculated settings.

Hodoscopes H_1 and H_3 measured points on the trajectory into M_{402} while H_4 and H_6 measured the trajectory out of the magnet. H_2 and H_5 measured vertical coordinates of the trajectory. Cerenkov counters C_1 and C_2 were used to reject pions. The recoil proton trajectory was measured in the horizontal plane by hodoscopes H_7 and H_8 while H_9 measured a vertical coordinate on the trajectory.

The t acceptance (Δt) was governed mainly by the size of the S_3 scintillator of width 15 cm positioned 16.25 m from the target. Δt varied from 0.12 (GeV/c)^2 at $|t| = 1.0$ to 0.175 at $t = 3.75$. The azimuthal acceptance $\Delta\phi$ was set by the size of the recoil counter R_1 for $|t| < 1.5$ (GeV/c)^2 and by the size S_3 for $t > 1.5$ (GeV/c)^2. Typical values were $\Delta\phi = 50$ mrad at $|t| = 1$ (GeV/c)^2 and $\Delta\phi = 25$ mrad at $|t| = 6$ (GeV/c)^2.

2.4. The monitors

A number of monitors were used for checks on the beam and for normalization of the data taken with target spin up to that with target spin down.

A thin parallel plate ionization chamber was used to measure the beam intensity per pulse. The charge deposited by the beam protons traversing six 1 cm cells of argon gas was collected on electrodes of 0.001 inch aluminium foil maintained at a collection voltage of 500 V. The charge was stored and integrated over a beam pulse in a Keithley 616 electrometer which digitised the information and read it out to a scalar. The beam intensity was calculated for the total charged stored, and agreed very well with a calibration against an irradiated aluminium foil [20].

A multiwire ionization chamber was used to measure the beam profile and position in both horizontal and vertical planes. The wire spacing was 1 mm and the charge collected by each wire over a beam pulse was stored on a capacitor. At the end of the pulse the capacitors were interrogated serially and the charge collected then displayed as a voltage level on an oscilloscope.

Two three scintillation counter telescopes viewed the target in the plane of target polarization; M_{135} above the scattering plane and M_{246} below. These two telescopes were sensitive to the number of protons hitting the target but insensitive to the polarization direction to the extent that strong interactions conserve parity. A third telescope $T_1T_2T_3$ was sited to view the target at 90° to the beam direction and was used for positioning the beam on the target.

Another good monitor was a small spectrometer arm mounted on a moveable table backwards of the polarized target. This arm was originally designed for the

measurement of spin asymmetries in inclusive scattering of pions and protons in the target fragmentation region and used scintillation counters B_1-B_3 in conjunction with a vertical bend in magnet M_{316}.

To act as a monitor the arm was set so that only protons scattered backwards of 90° were detected. Such protons could only have come from the complex nuclei in the target and thus was not sensitive to the polarization sign.

3. Electronics and data acquisition

3.1. Trigger logic

The logic used to define a trigger was very simple. The forward arm ($S_1S_2S_3S_4$) and recoil arm (R_1R_2) coincidences were formed separately and then brought together to form the final RS trigger. Short resolving times (<5ns) helped to reject fast pions. The status of the Čerenkov counters C_1 and C_2 was recorded in a parallel pattern unit (PPU).

Each photomultiplier in each hodoscope was cabled to a separate input of a serial pattern unit (SPU). Signals from the hodoscope element set flip-flops in the SPUs whenever they were in time coincidence with a gate derived from the trigger pulse. In addition the SPU formed a fast OR output of all the input pulses which was put into coincidence with the trigger gate to form a CANDIDATE pulse. A CANDIDATE signal was defined as an event with at least one particle in each of a specified number of hodoscopes. The CANDIDATE signal provided an interrupt to the on-line computer and started the data-acquisition phase.

The CANDIDATE initiated the encoding phase, where the hodoscope pattern was clocked into the encoding SPADAC [21] buffer at 10 MHZ. The addresses of up to two hits in each hodoscopes could be encoded, the data from the nine hodoscopes occupying only nine 16-bit computer words.

The details of encoding with the SPADAC system have been discussed previously [21]. On completion of the encoding phase the nine hodoscope data words and a tenth word from the PPU used to describe the Cerenkov status of an event, were transferred to the Nova. At the end of each burst the contents of 24 CAMAC scalars were transferred. When a data buffer was full, the event blocks it contained were pre-analysed and the information written to a disk so that the performance of the equipment could be monitored. Then the buffer was written to tape.

An on-line program calculated the forward particle momentum, coplanarity and recoil angle for each event and periodically displayed histograms of these quantities and of the hodoscope distributions. The on-line analysis indicated that elastic events were being acquired and that the apparatus was performing satisfactorily.

3.2. Data taking procedure

In order to increase the elastic signal, the counters S_3 and S_4 were omitted from the forward arm coincidence, thereby enlarging the acceptance, and the loose trigger

$[R_1R_2]$ $[S_1S_2]$ used. It was found that running in this mode did not unduly increase the level of background under the signal compared to the tight trigger conditions $[R_1R_2]$ $[S_1S_2S_3S_4]$.

All data for $|t| > 1.8$ (GeV/c)^2 was taken with the loose trigger except for $|t| = 2.75$ (GeV/c)^2 where the currents in the steering magnets were zero and so had no effect in separating signal and background. The tight trigger was used for this situation and for points with $|t| < 1.8$ (GeV/c)^2 where the elastic event rate was high.

The data taking rate was strongly t dependent because of the steeply falling elastic cross section with increasing t and the acceptance of the spectrometer. At $|t| = 1.6$ (GeV/c)^2 a run of duration one hour yielded typically 5×10^3 triggers while at $|t| = 5$ (GeV/c)^2 only 100 triggers were obtained.

As discussed above different beam conditions were set up to reduce radiation damage to the target. Most data was taken with a ramped beam, the rest with a small beam. The ramped beam increased the vertical beam divergence and spot size and broadened the elastic coplanarity signal by about 5% but gave a negligible decrease in signal to background ratio and extended the lifetime of the target by a factor of 3.

A series of runs with polarization sign reversals of the form +−−++−−+ up to 10 reversals were made in order to maximise the number of +/− pairs and to reduce the errors from difts and systematic effects. Frequently a data set at a particular $|t|$ value was repeated a few days later as a consistency check.

4. Data analysis

The off-line data analysis was performed on the Rutherford Laboratory IBM 360/195 computer.

Selected runs from the raw data tapes were copied onto a master data tape. The analysis program searched the tape for selected runs and analysed each event within that run. It decoded the SPADAC words to obtain the address of the struck element in each hodoscope, calculated the forward particle momentum and angle, recoil angle and coplanarity and printed histograms for these quantities. Scatter plots of momentum and recoil angle and of forward angle and recoil angle were also produced. At all settings the elastic events were clearly visible and subsequent analyses were made to investigate the effects of cuts made on the various distributions.

4.1. Event selection

In all data sets the elastic signal was clearly visible in the raw data. Fig. 3 shows distributions in recoil angle correlation θ_R and forward momentum P_f at three different t values. The observed resolution of the elastic peaks agreed quite well with the calculated values which took into account Coulomb scattering, beam size

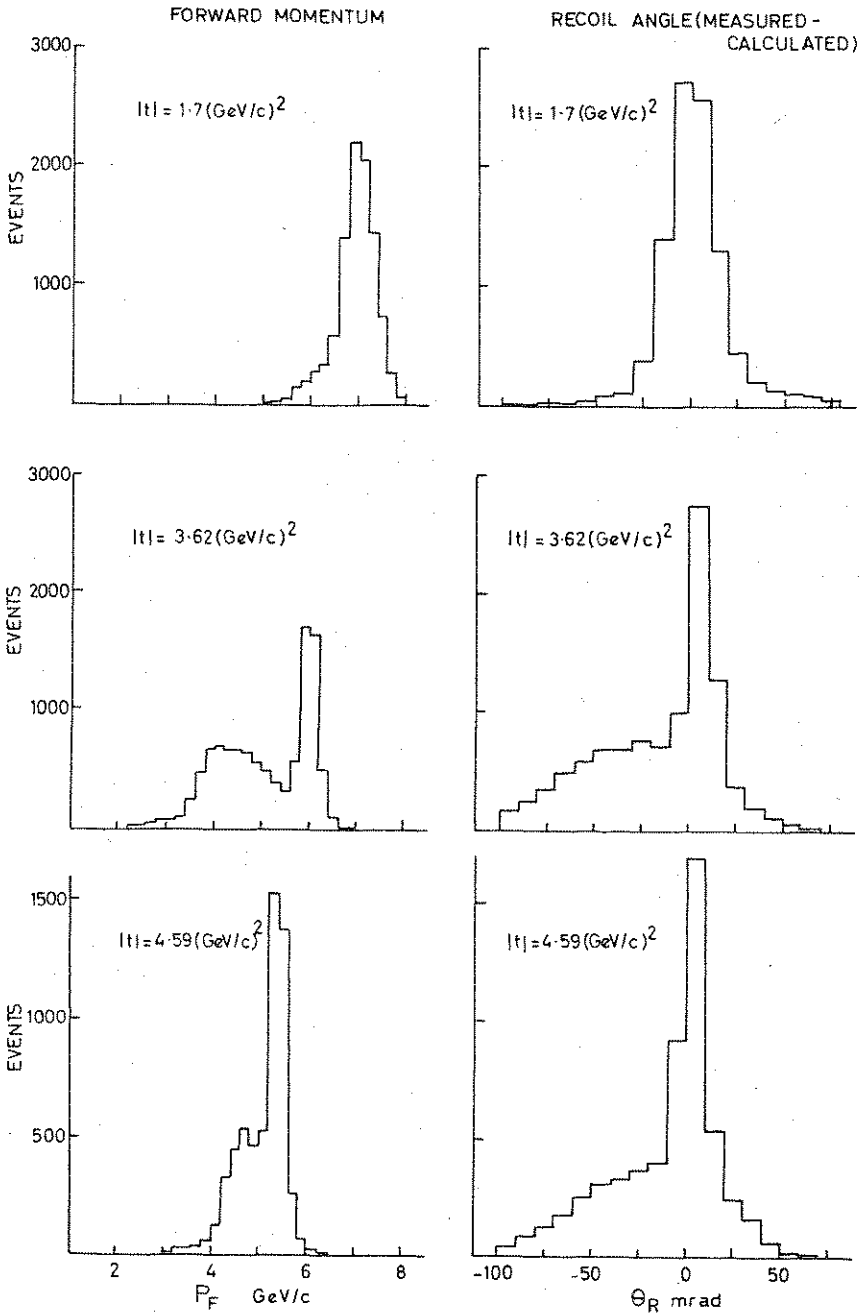

Fig. 3. Distributions in angle-angle correlation θ_R and forward momentum P_f at $|t| = 1.7$, 3.62 and 4.59 $(GeV/c)^2$.

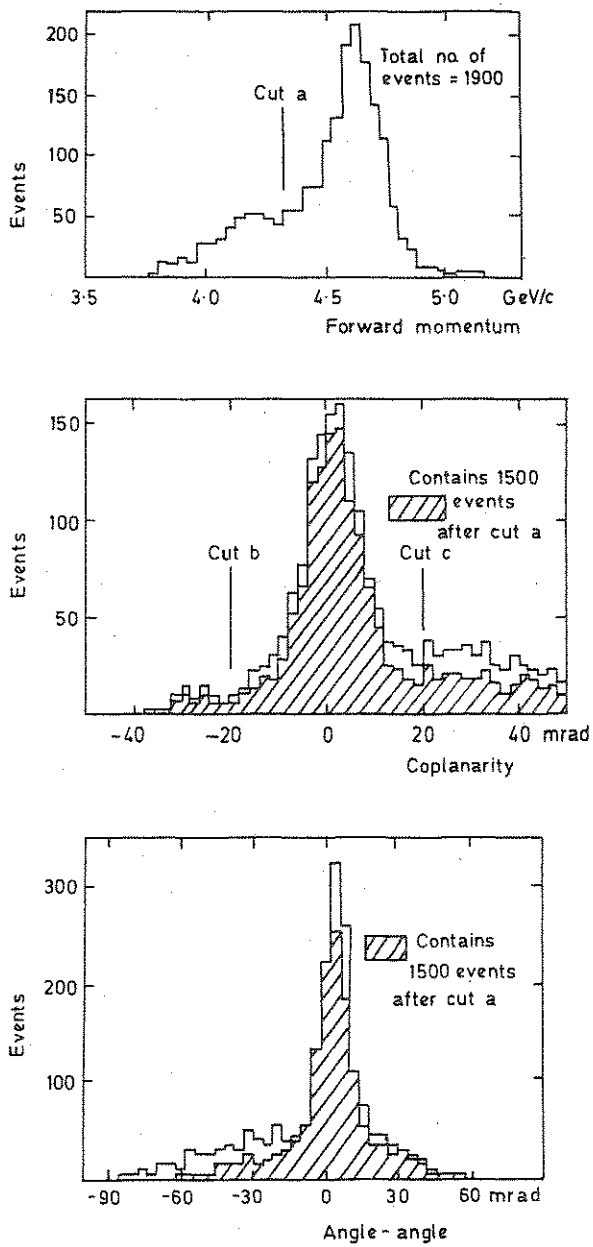

Fig. 4. Distributions in forward momentum, coplanarity and angle-angle correlation at $|t| = 6$ $(GeV/c)^2$. The cross hatched distributions show the effect of making the forward momentum cut 'a'.

and divergence and width of hodoscope elements. Before extracting the elastic signal, the background level under the peak in the θ_R distribution was minimised by making a cut on the forward momentum and two cuts on the coplanarity for each event. The cuts made for the case of $|t| = 6$ (GeV/c)^2 are shown in fig. 4.

That the events left in the peak are due to scattering from free hydrogen and not contaminated by quasi-elastic scatters from bound protons was further demonstrated by analysing runs made with a carbon target. No peak occurs and the background in the distribution from propanediol is well described by the carbon data.

The background subtraction was made after summing the final histograms from a number of runs. The low level of the backgrounds made it unnecessary to fit them separately for each run so all the runs in a data set were summed and the tails of the distribution fitted with a polynomial (usually a quadratic) using a least squares method. The resulting shape was then scaled to fit the tails of the distribution obtained by summing those runs in the data set which had target polarization positive. The background level per bin under the peak was estimated by extrapolating the fitted curve and subtracting from the signal to give the number of hydrogen events N_H^+ present and associated error δN_H^+. An identical procedure gave N_H^- and δN_H^-.

4.2. Calculation of the asymmetry

The elastic scattering asymmetry was calculated from

$$A_H = \frac{N^+ - fN^-}{N^+ + fN^- - (B^+ + fB^-)}$$

$$= \frac{N^+ - fN^-}{N_H^+ + fN_H^-} ,$$

where the background $B^\pm$ is unpolarized, and where

$$f = \frac{\text{number of incident protons for positive } P_T}{\text{number of incident protons for negative } P_T} .$$

The monitors for measuring this factor have already been described, and in general the average value from all the monitors was used for f.

If A_H is small then the error δA_H is given by

$$\delta A_H \approx [(\delta N^+)^2 + f^2(\delta N^-)^2 + (N^-)^2 \delta f^2]^{1/2}/(N_H^+ + fN_H^-) .$$

The contribution to the error in f, δf was from systematic effects such as drifts in counter efficiency. δf was calculated from the spread of the ratios calculated with each monitor about their mean. A figure of merit for each monitor was also calculated to indicate the size of drift for that monitor. A final consistency check was made by using an internal monitor, the tails of the θ_R distribution. As the background in the tails came from the unpolarized nucleons of the complex nuclei the

asymmetry

$$A_{\text{tails}} = \frac{T^+ - fT^-}{T^+ + fT^-}$$

was required to be zero, where $T^\pm$ are the number of events in the tails. Data sets with A_{tails} differing from zero by more than two standard deviations were rejected.

The polarization parameter P_0 was obtained from the equation

$$P_0 = \frac{A_H}{\langle P_T \rangle} = \frac{A_H}{\frac{1}{2}[(\langle P_T^+ \rangle + \langle P_T^- \rangle) - A_H(\langle P_T^+ \rangle - \langle P_T^- \rangle)]} ,$$

$$\delta P_0 = \frac{\delta A_H}{\langle P_T \rangle} ,$$

where

$$\langle P_T^+ \rangle = \sum_i (P_T^+)_i / n^+ ,$$

$$\langle P_T^- \rangle = \sum_i (P_T^-)_i / n^- ,$$

and n^+ are total number of runs with polarization sign +, n^- are total number of runs with polarization sign −, and $(P_T)_i$ is the average target polarization (corrected for radiation damage) in the ith run.

In addition there is an overall systematic uncertainty of 5% due mainly to the uncertainty in the knowledge of the absolute value of target polarization.

5. Results and discussion

The measured polarizations at 7.9 GeV/c are shown in fig. 5 and tabulated in table 2. These data show the structure which is characteristic of the higher momenta; the polarization always being zero or positive. The value of the polarization rises from zero at $|t| = 1.0$ (GeV/c)^2 to a peak at $|t| = 1.7$ (GeV/c)^2 and then falls to zero again at $|t| = 2.0$ (GeV/c)^2. There is some indication of a third peak at $|t| = 2.8$ (GeV/c)^2. There is no compelling evidence for further structure above $|t| = 3.25$ (GeV/c)^2.

Fig. 6 shows a comparison of the present data with that at 7.0 GeV/c [7], 10 GeV/c [5], 12 GeV/c [8,23], and 17.5 GeV/c [5]. This comparison shows that the 7.9 GeV/c data is similar in structure to that of the data at higher beam momentum but differs from that at 7.0 GeV/c. At 7.0 GeV/c there is no indication of the dip at $|t| = 2.0$ (GeV/c)^2 which by 7.9 GeV/c has appeared. This behaviour of the amplitudes appears also to be reflected in the differential cross sections where 7.0 GeV/c is at the threshold of a change in the shape of the differential cross section.

The overall shape of the 7.9 GeV/c data is in agreement with that of

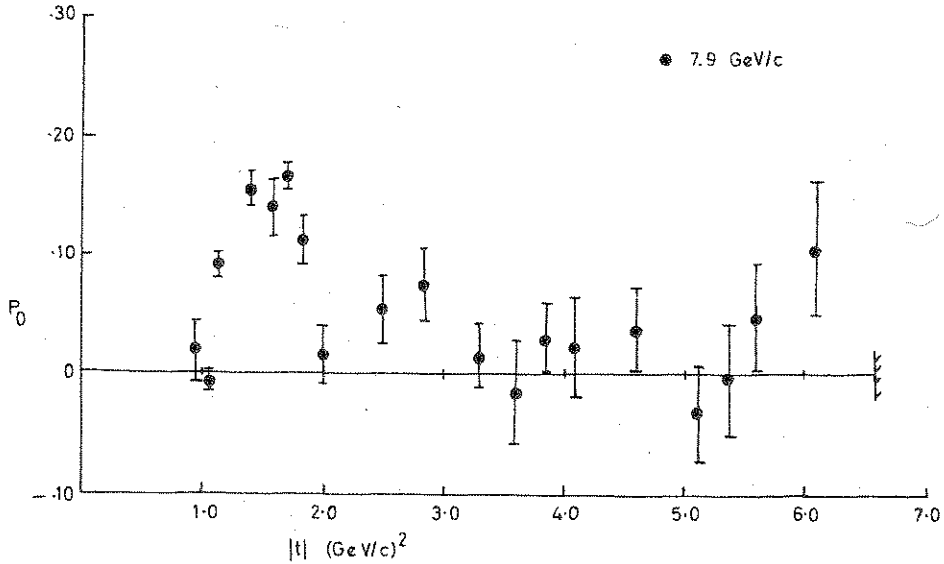

Fig. 5. The polarization parameter at 7.9 GeV/c as a function of four-momentum transfer squared, $-t$.

Table 2

Polarization parameter in pp elastic scattering at 7.9 GeV/c

$\|t\|$ (GeV/c)^2	P_0
0.94	0.018 ± 0.024
1.05	−0.006 ± 0.008
1.14	0.092 ± 0.010
1.39	0.156 ± 0.015
1.59	0.140 ± 0.023
1.70	0.167 ± 0.011
1.84	0.112 ± 0.021
2.01	0.015 ± 0.024
2.51	0.054 ± 0.028
2.85	0.077 ± 0.032
3.33	0.015 ± 0.027
3.62	−0.015 ± 0.043
3.86	0.029 ± 0.030
4.10	0.023 ± 0.042
4.59	0.037 ± 0.034
5.12	−0.033 ± 0.040
5.38	−0.004 ± 0.047
5.60	0.048 ± 0.046
6.10	0.107 ± 0.057

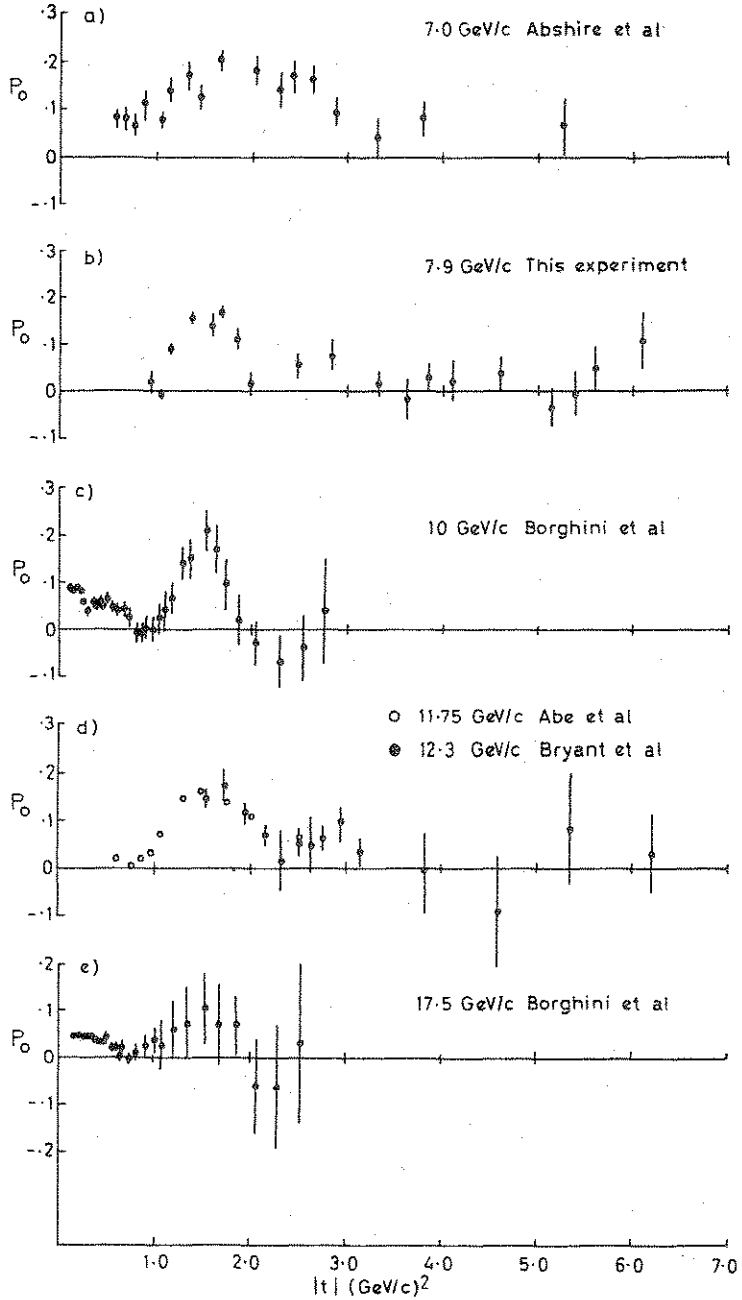

Fig. 6. Comparison of polarization data at (a) 7.0 GeV/c, (b) 7.9 GeV/c, (c) 10 GeV/c, (d) 12 GeV/c and (e) 17.5 GeV/c as a function of four-momentum transfer squared, $-t$.

Borghini et al. [5] at 10, 14, and 17.5 GeV/c; particularly in that P_0 falls to around zero at $|t| = 2.0$ (GeV/c)^2. That this is not so at 12 GeV/c is pointed out below.

It should be emphasized that some of the published values from Borghini et al. are incorrect and that the correct values are tabulated in the unpublished errata given in ref. [5].

It is interesting to consider the variation of the polarization with the square of the c.m. energy s and fig. 7 shows this at $|t| = 0.3$ (GeV/c)^2 the first peak, at $|t| = 1.7$ (GeV/c)^2 the second peak and at $|t| = 2.0$ (GeV/c)^2 the second double zero. At $|t| = 0.4$ (GeV/c)^2 the data lie on a smooth curve, P_0 falling approximately as s^{-1}. At $|t| = 1.7$ (GeV/c)^2 P_0 is essentially s independent. For $|t| = 2.0$ (GeV/c)^2 the rapid change between $s = 13.25$ and 14.9 GeV^2 (beam momenta of 7.0 and 7.9 GeV/c respectively) is evident. At $s = 22.5$ GeV^2 (beam momentum 12 GeV/c) there is a noticeable deviation from the general trend of the higher s data. The two experiments in this region [8,23] show that the second peak has widened allowing P_0 at $|t| = 2.0$ (GeV/c)^2 to be close to the peak value.

In fact an extension of the experiment of ref. [23] by Miettinen et al. [25] shows quite conclusively that, at 11.75 GeV/c at least, P_0 falls slowly away from the peak value and does not fall to zero at $|t| = 2.0$ (GeV/c)^2.

A wide variety of models have been used to try and fit and interpret these features of the polarization together with the differential cross sections. These models generally fall within the three categories of Regge pole, geometrical or eikonal descriptions of the scattering process.

The structure at small t ($t \lesssim 1.5$ (GeV/c)^2) can be reproduced using a conventional Regge approach with pole exchange alone, but it is not possible to obtain satisfactory fits to both the differential cross sections and polarizations or reproduce the s dependence of the polarization. The introduction of strong cuts due to rescattering or absorption effects enables the observed experimental features to be reproduced at least for $|t| \lesssim 1$ (GeV/c)^2. For example the model of Kane and Seidl [11] shows how the dip in P_0 at $|t| = 0.8$ (GeV/c)^2 develops with s to become a double zero and to eventually go negative.

Geometrical descriptions of the nucleon-nucleon interaction by the use of optical models have been quite successful. In such models the interaction is assumed to be diffractive and Durand and Halzen [14] have shown that if one makes two additional assumptions then a simple relation between polarization and differential cross section is obtained. The assumptions are that the only spin dependence of the interaction arises from a weak spin orbit force and that the spin flip amplitude peaks at the periphery of the non-flip amplitude. Then the relation is

$$P_0 \frac{d\sigma}{dt} \approx \frac{d}{d\sqrt{-t}} \frac{d\sigma}{dt} .$$

Thus structure in the polarization is expected at the four-momentum transfers at

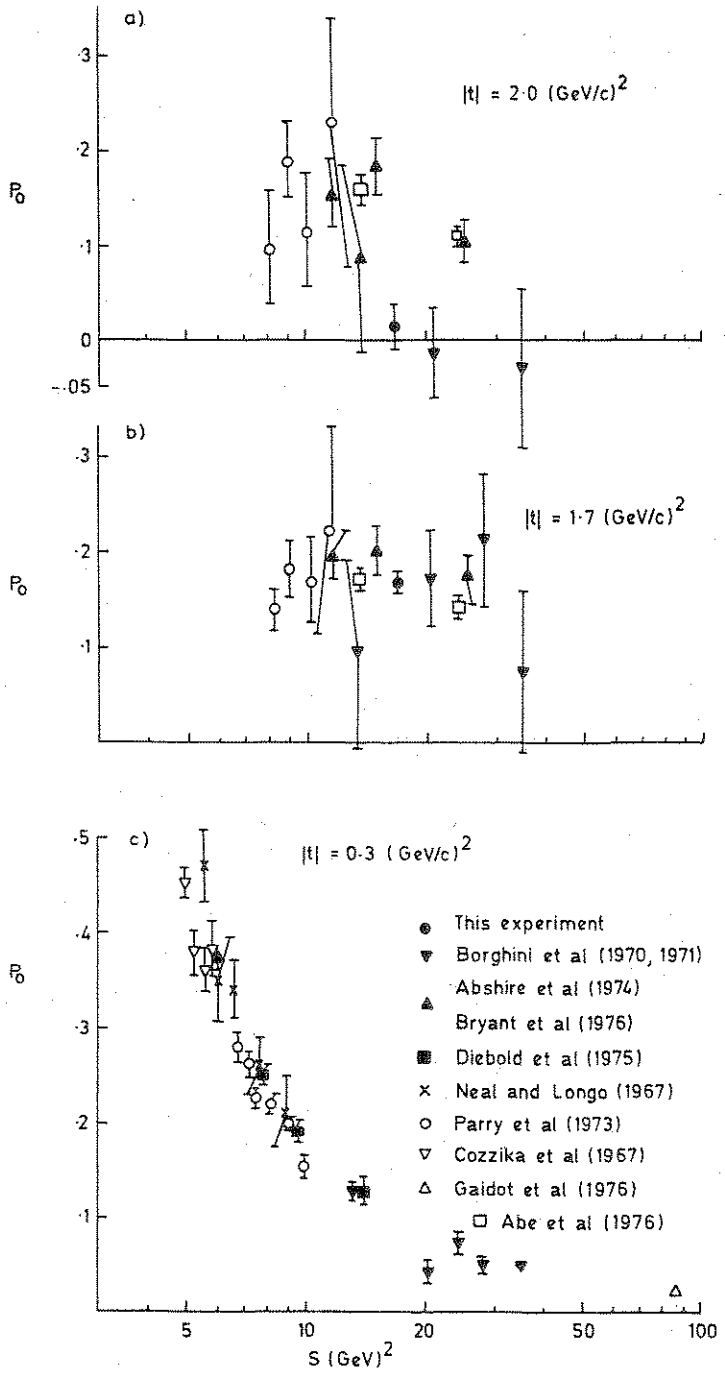

Fig. 7. Comparison of polarization as a function of c.m. energy squared, s at (a) $|t| = 2.0$ (GeV/c)^2, (b) $|t| = 1.7$ (GeV/c)^2 and (c) $|t| = 0.3$ (GeV/c)^2.

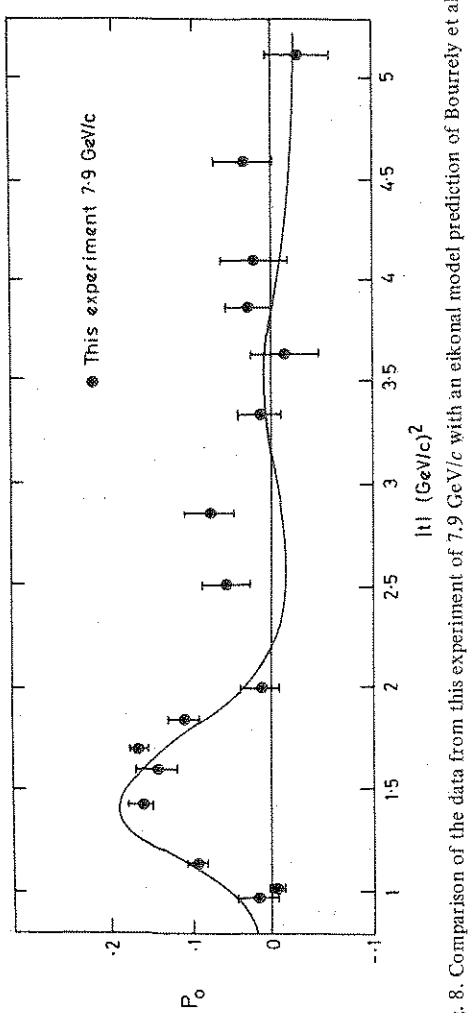

Fig. 8. Comparison of the data from this experiment of 7.9 GeV/c with an eikonal model prediction of Bourrely et al. [12].

which the differential cross section also exhibits structure.

A particular model is that of Chu and Hendry [13] where the picture is of scattering from a grey absorbing disc with radius $R \approx 0.9$ fm. This gives a polarization

$$P_0 \approx [J_1(R\sqrt{-t})]^2/R\sqrt{-t}\,,$$

with double zeros located at the zeros of the Bessel function at $|t| = 0.7$, 2.5 and 5.2 (GeV/c)^2. This is in very good agreement with the data at 12.3 GeV/c out to $|t| = 6$ (GeV/c)^2.

However as the differential cross section for both pp and pn elastic scattering are approximately equal all such models must predict the polarizations for the two reactions to be the same. That this is not the case is obvious from the data of Diebold et al. [15].

Attempts have been made to unify the s and t channel descriptions of nucleon-nucleon scattering by using the eikonal approach together with Regge pole exchange. In a model such as that of Bourrely et al. [12] the geometrical description of nucleons which leads to a multiple scattering series is combined with Regge pole exchange with absorption. With such an approach, a reasonable description of polarizations in nucleon-nucleon scattering has been obtained over a large range of energy and four-momentum transfer. Fig. 8 shows the predictions from this model for pp elastic scattering at 7.9 GeV/c compared to the data from this experiment. There is good agreement out to approximately $|t| = 2$ (GeV/c)^2.

We wish to thank M. Borghini and the CERN polarized target group for their help in setting up a CERN target at the Rutherford Laboratory and A. Thompson and C. Thomas and the Rutherford Support staff for keeping it operational. Also N.E. Booth and H. Beaumont who participated in the early phase of the experiment. The technical support of J. Bibby, W. Huta, A. Kupferschmid and A. Looten is gratefully acknowledged.

References

[1] P. Grannis et al., Phys. Rev. 148 (1966) 1297.
[2] G. Cozzika et al., Phys. Rev. 164 (1967) 1672.
[3] H.A. Neal and M.J. Longo, Phys. Rev. 161 (1967) 1374.
[4] M. Borghini et al., Phys. Letters 24B (1967) 77.
[5] M. Borghini et al., Phys. Letters 36B (1971) 501; 31B (1970) 405; Polarization in hadron-proton elastic scattering at 10, 14 and 17.5 GeV/c (Errata and New Data Tables) CERN preprint (January 1972).
[6] J.H. Parry et al., Phys. Rev. D8 (1973) 45.
[7] G.W. Abshire et al., Phys. Rev. Letters 32 (1974) 1261.
[8] G.W. Bryant et al. Phys. Rev. D13 (1976) 1.
[9] D.M. Austin, W.H. Greiman and W. Rarita, Phys. Rev. D2 (1970) 2613.
[10] V. Barger and R. Phillips, Phys. Rev. Letters 20 (1968) 564; 22 (1969) 16.

[11] G.L. Kane and A. Seidl, Rev. Mod. Phys. 48 (1976) 365.
[12] C. Bourrely, A. Martin and J. Soffer, Eikonal description of nucleon-nucleon polarization, Saclay preprint, 1976.
[13] S.-Y. Chu and A.W. Hendry, Phys. Rev. D6 (1972) 190;
T.Y. Cheng, S-Y. Chu and A.W. Hendry, Phys. Rev. D7 (1973) 86.
[14] L. Durand and F. Halzen, Nucl. Phys. B104 (1976) 317.
[15] R. Diebold et al., Phys. Rev. Letters 35 (1975) 632.
[16] F. Aitchison and J. Butterworth, Rutherford Laboratory report, RL-73-112, 1973.
[17] P. Roubeau et al., Nucl. Instr. 82 (1970) 323.
[18] M. Borghini et al., Nucl. Instr. 84 (1970) 168.
[19] H.R. Petri and G.W. Abshire, Nucl. Instr. 119 (1974) 205.
[20] J.B. Cumming, Ann. Rev. Nucl. Sci. 13 (1963) 261.
[21] L. Dick et al., Nucl. Phys. B43 (1972) 522.
[22] A. Gaidot et al., Phys. Letters 61B (1976) 103.
[23] K. Abe et al., Phys. Letters 63B (1976) 239.
[24] A. Gonidec, A. Kupferschmid and K. Kuroda, Nucl. Instr. 137 (1976) 387.
[25] H.E. Miettinen et al., University of Michigan preprint UM HE 77-6.